Article

Preparation and Tribological Behavior of Nitrogen-Doped Willow Catkins/MoS₂ Nanocomposites as Lubricant Additives in Liquid Paraffin

Yaping Xing [1], Ebo Liu [1], Bailin Ren [1], Lisha Liu [1], Zhiguo Liu [1], Bocheng Zhu [1], Xiaotian Wang [1], Zhengfeng Jia [1,*], Weifang Han [1,*] and Yungang Bai [2]

[1] School of Materials Science and Engineering, Liaocheng University, Liaocheng 252059, China
[2] Shandong Qichanxintu Composite Material Co., Ltd., Liaocheng 252800, China; bai9521@hotmail.com
*   Correspondence: jiazhfeng@lcu.edu.cn (Z.J.); hanweifang@lcu.edu.cn (W.H.)

Abstract: In this study, willow catkins/MoS₂ nanoparticles (denoted as WCMSs) have been prepared using a hydrothermal method. The WCMSs were modified with oleic acid (OA) to improve dispersion in base oil. The friction and wear properties of WCMSs in liquid paraffin (LP) for steel balls were investigated using a four-ball wear tester. The results have shown that at a high reaction temperature, willow catkins (being used as a template) and urea (being used as a nitrogen resource) can effectively decrease the wear scar diameters (WSDs) and coefficients of friction (COFs). At a concentration of 0.5 wt.%, the WSD and COF of steel balls, when lubricated using LP containing modified WCMS with urea, decreased from 0.65 mm and 0.175 of pure LP to 0.46 mm and 0.09, respectively. The addition of urea and hydroxylated catkins can generate a significant number of loose nano-sheets and even graphene-like sheets. The weak van der Waals forces, decreasing the shear forces that the steel balls must overcome, provide effective lubrication during rotation. On the other hand, the tribo-films containing MoS₂, FeS, azide, metal oxides and other compounds play important roles in reducing friction and facilitating anti-wear properties.

Keywords: willow catkins; MoS₂; hydrothermal; urea; wear

1. Introduction

Nanomaterials are widely studied because of their excellent properties with respect to tribology, notably in reducing friction, enabling wear resistance, with significant implications for environmental protection [1–3]. Two-dimensional (2D) nanomaterials, including BN, graphene, and MoS₂ exhibit superior tribological properties because of their distinct layer structures and self-lubricating ability [3,4]. Weak van der Waals forces between the adjacent lamellae decrease the shear stress during sliding [2]. Liquid exfoliation and hydrothermal reaction are two standard procedures in the fabrication of MoS₂ nanosheets [5,6]. Ion intercalation and exchange by sonication in solution are often used in exfoliation methods [5]. In the case of the hydrothermal route, the nature of the solution, temperature, and hybrid elements can be adjusted to improve material properties [2,7,8]. With the objective of improving the tribological properties of MoS₂, composites including MoS₂/carbon [7,9], metal oxide/MoS₂ [10], and boron nitride/MoS₂ [1] have been investigated to tune possible synergistic effects. Wu et al. [7] have synthesized a series of MoS₂@carbon nanocomposites using a hydrothermal method, and noted a synergism between the MoS₂ and carbon nanocomposites that resulted in improved dispersibility and tribological properties relative to the individual components. Furthermore, MoS₂ nanoparticles grown on carbon nanotubes, graphene, and fullerene C60 were executed using a simple solvothermal method. On the other hand, surface functionalization and elemental doping of nanoparticles can further improve the dispersion stability and chemical activity in base oil (mineral oil, such as engine oil and/or liquid paraffin), and their tribological behaviors in lubricants can be

enhanced due to the tribochemical reactions between these functional groups/doped atoms and the friction surface [1,9]. Various dispersants and surface-active chemicals, including alkylamines, alkanethiols, organic acid, and amine were used for the functionalization of nanostructured and doped elements, respectively [9].

Willow catkins (denoted as WCs), the willow flowers in spring, are widely dispersed by wind and cause damage to the environment due to their high specific surface area and facile spontaneous combustion [11,12]. Direct combustion of catkins results in environmental pollution with the release of CO_2 and NOx [11]. Many researchers have addressed the practical use of renewable biomass materials, including catkins, celtuce leaves, and seed shells [11,13,14]. The pyrolysis of these biomass materials generates carbon materials and the possible fabrication of composites represents a reuse of catkins [15–17]. Zhang et al. [18] generated N/S co-doped carbon micro-tubes by the pyrolysis of catkins in an inert atmosphere. The resultant hybrids exhibited superior electrocatalytic properties when compared with commercial products. While this work offers a means of reusing catkins in treating environmental pollution and water contamination, the associated energy consumption represents a challenge in terms of sustainability. So far, authors did not find any research on the composites of willow catkins and MoS_2 being used as lubricant additives.

In this study, willow catkins and urea have been used as matrix and nitrogen resource, respectively, to prepare nitrogen-doped willow catkins/MoS_2 nanocomposites using hydrothermal methods. The composites have been modified with OA to enhance the dispersibility in LP to evaluate tribological properties using a four-ball wear tester [19]. The wear mechanism of the composites has also been investigated.

2. Materials and Methods

2.1. Materials and Preparation

Sodium molybdate dihydrate, thioacetamide, oleic acid and NaOH were purchased from the Aladdin Biochemical Technology Company (Shanghai, China) and used as supplied. The LP (viscosity: 258.56 mm^2/s (40 °C), flash point: 279 °C, pour point: −15 °C) was obtained from Liaocheng Manxiandi lubricating oil company (Liaocheng, China) and used without treatment. AISI-52100 steel balls (Ø12.7 mm) were employed in the four-ball wear tester. The willow catkins were collected from the campus of Liaocheng University.

The willow catkins were washed sequentially with tap water and deionized water, transferred into a NaOH solution (2.0 wt.%) with vigorous stirring for 24 h, then centrifuged and washed to achieve well-dispersed hydroxylated willow catkins solutions. Sodium molybdate dihydrate (1 g) and thioacetamide (1 g) were added to the hydroxylated willow catkins solution (30 mL) with stirring, then transferred into the hydrothermal reactor. The solution was heated above 100 °C for 24 h to obtain the composites ($WC_3M_1S_1$). For the purposes of comparison, particles different percentages of molybdate dihydrate and thioacetamide, with/without willow catkins and urea were also synthesized (see Table S1).

The modification and wear experiments using WCMSs have been outlined in previous papers [19]. The LP containing OA-modified WCMSs (code as OAWCMSs and with concentrations of 0.2, 0.5, 1.0, 1.5, and 2.0 wt%, respectively) were stable within 7 days (see Figure S1). Wear experiments were conducted using a MRS-10A four-ball wear tester of Jinan Shunmao Experimental Technology Company in China (392 N load, 1450 rpm, and 30 min).

2.2. Characterization

The microstructure of the composites was assessed using a JEM-2100 high-resolution transmission electron microscope (HRTEM) and a SIGMA500/VP field-emission scanning electron microscope (FE-SEM) equipped with energy-dispersive X-ray analysis (EDXA, Kevex Sigma, USA). The X-ray diffraction (XRD) patterns were collected on a Bruker D8 Advanced X-ray Diffractometer using Cu Kα radiation in the 2θ range between 10° and 80° with a scanning rate of 8° min^{-1}. The ESCA LAB Xi+ X-ray photoelectron spectrometer

(XPS) and Bruck IFs66v spectrometer were used to collect X-ray photoelectron spectra and Fourier transform infrared (FT-IR) spectra of the composites and/or worn surfaces, respectively. Al-Ka radiation was used as the excitation source to determine the binding energies of the target elements at a pass energy of 29.4 eV and a resolution of ± 0.2 eV. The binding energy of C1s (284.5 eV) was used as the internal reference for XPS analysis. Thermogravimetric analysis (TGA) was conducted using a NETZSCHSTA499 simultaneous thermal analyzer, operating from room temperature to 800 °C at a heating rate of 10 °C/min in N_2.

3. Results and Discussion

3.1. Results

Representative FE-SEM and TEM images of WCMSs produced at different hydrothermal temperatures are presented in Figure 1. It can be seen that the MoS_2 nano-sheets increase in size and become closely clustered on raising the hydrothermal temperature from 120 °C to 200 °C, where the thickness of the nano-sheets was less than 100 nm (Figure 1a,b). The mapping images show that MoS_2 sheets are strongly attached on the surfaces of willow catkins (Figure S2). The elliptic holes exhibit a major axis of 5 μm and both sides of the entocoele are strongly attached with MoS_2 nano-sheets (Figure 1c). The thickness of these nano-sheets is still less than 100 nm (Figure 1c,d). The TEM analysis has established that the willow catkins were covered with MoS_2 and the interlayer spacing between the nano-sheets was ca. 0.65 nm (Figure 1e,f).
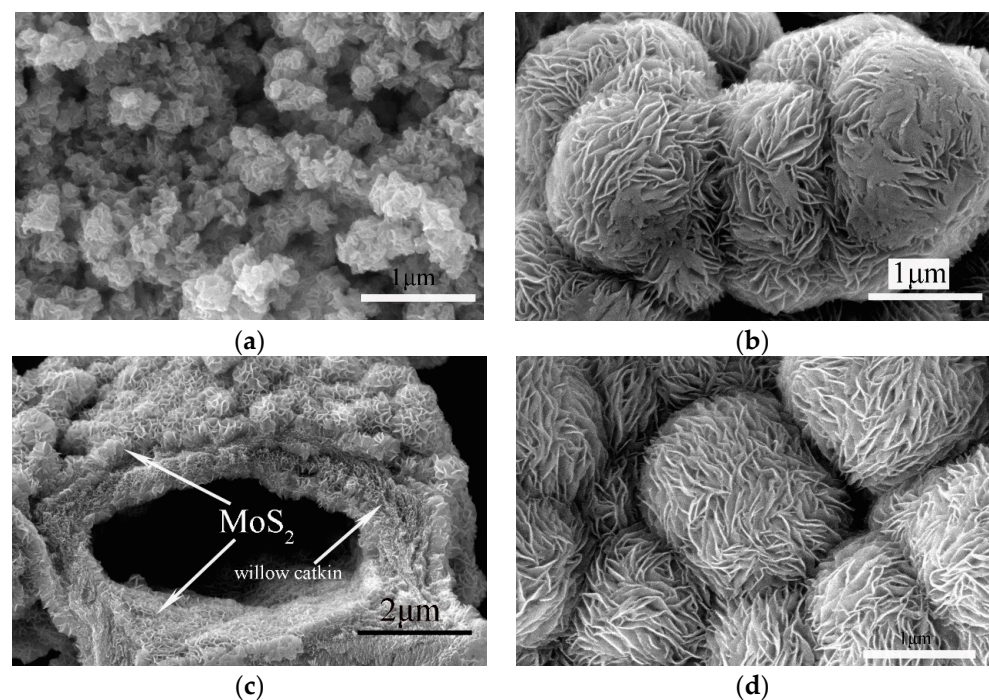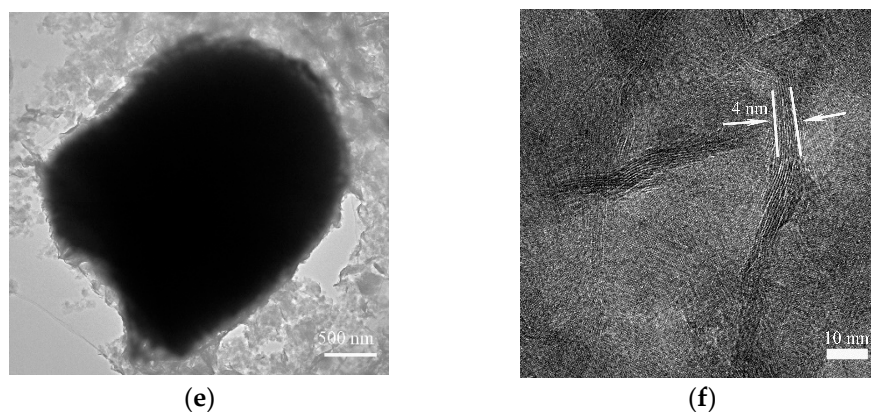

Figure 1. *Cont.*

| (e) | (f) |

Figure 1. FE-SEM images of $WC_0M_2S_1$ produced at a hydrothermal temperature of 120 °C (**a**) and 200 °C (**b**). FE-SEM (**c,d**) and TEM (**e,f**) images of $WC_2M_2S_1$ at a hydrothermal temperature of 200 °C.

The XRD patterns and Raman spectra of $WC_2M_2S_1$ generated at a hydrothermal temperature of 120 °C and 200 °C, respectively, are presented in Figure 2. The diffraction peaks at 13.89°, 33.42°, 38.87°, 48.32°, and 58.91° can be attributed to (002), (100), (103), (105), and (008) crystal planes, respectively, establishing a hexagonal MoS_2 structure (card No. 37-1492) [20]. An increase in hydrothermal temperature is accompanied by sharper diffraction peaks with increased intensity, indicating improved the growth of MoS_2 crystals along (002) plane and (100) plane, respectively [21]. The Raman spectra presented in Figure 2b–d were obtained using a laser irradiation wavelength of 532 nm. The peaks at 376.48 cm^{-1} and 402.26 cm^{-1} are attributed to the E^1_2g and A^1g modes of MoS_2, suggesting in-layer vibration of S and Mo atoms and outer layer vibration of S atoms along the c axis, respectively [21,22]. Furthermore, the distance value of the E^1_2g and A^1g peaks is 25.65 cm^{-1}, which is smaller than the value (26.3 cm^{-1}) for bulk MoS_2. The lower E^1_2g and A^1g peak distances indicate a decrease in the number of layers [21], which results from the use of willow catkins. The Raman peak at 819.88 cm^{-1} is assigned to the vibration of MoO_3, possibly suggesting a transfer of MoO_3 into MoS_2 as the hydrothermal temperature was increased from 120 °C to 200 °C [20]. The D and G peaks of carbon (at 1380 cm^{-1} and 1600 cm^{-1}) were not observed after hydrothermal treatment [21].



| (a) | (b) |

Figure 2. *Cont.*

(c)

(d)
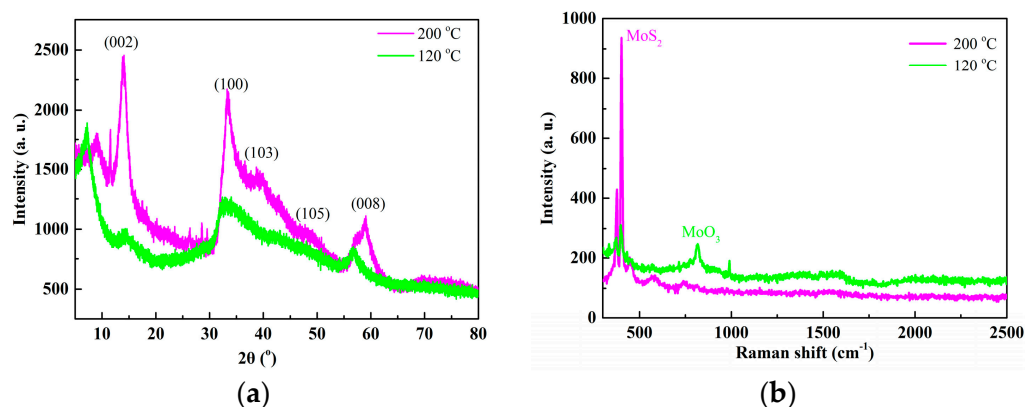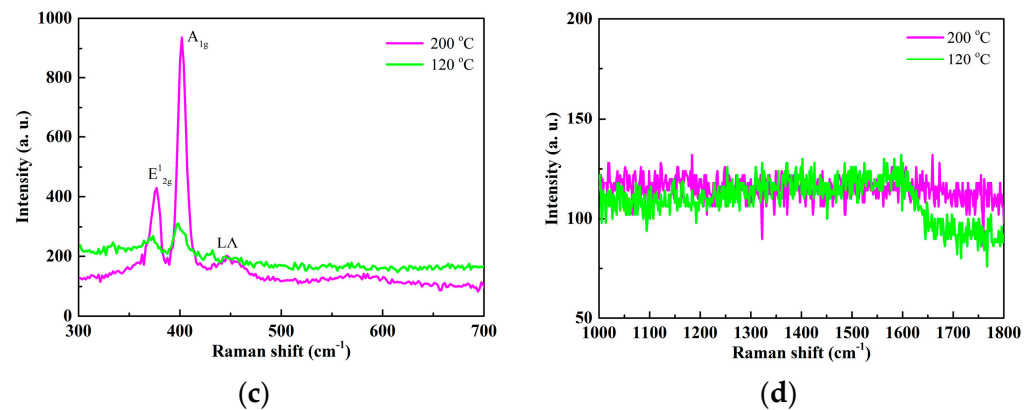
Figure 2. XRD patterns (**a**) and Raman spectra (**b**–**d**) for $WC_2M_2S_1$ produced at a hydrothermal temperature of 120 °C and 200 °C, respectively.

The FT-IR spectrum of $WC_2M_2S_1$ (Figure 3a) shows a broad peak at ca. 3200 cm^{-1}, attributed to -OH and/-NH$_2$ on the surface of willow catkins [23]. Peaks at ca. 1139 cm^{-1} and 888 cm^{-1} are assigned to Mo-O and S-S bonds, respectively [8]. The peaks at ca. 1017 cm^{-1} and 1418 cm^{-1} are due to C-O-C and -COO- groups, respectively [23]. A weak peak at ca. 695 cm^{-1} is assigned to the Mo-S bond [24]. The peak at ca. 1611 cm^{-1}, attributed to C=N and/or C=C groups, suggests the presence of aromatic rings associated with willow catkins [11]. The TGA curves (Figure 3b) have revealed weight losses for $WC_2M_2S_1$ before and after modification of 8.5% and 25.1%, respectively [19].

(a)

(b)
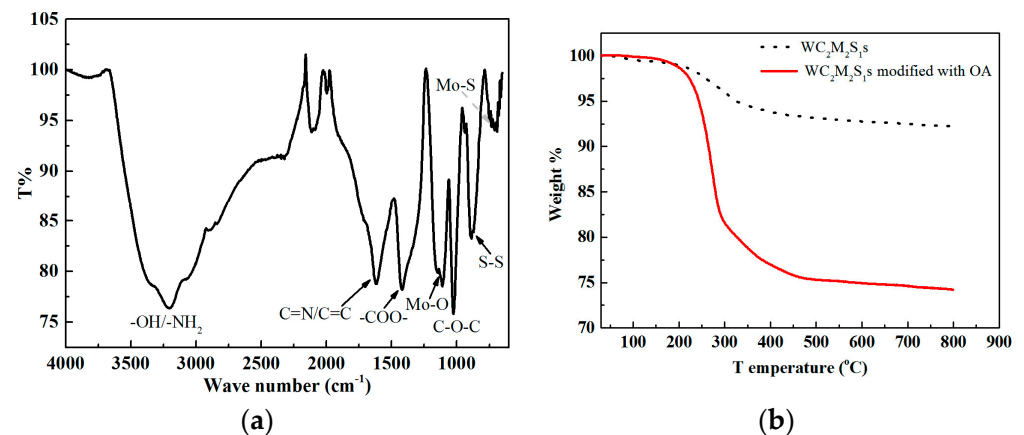
Figure 3. (**a**) FT-IR spectrum of $WC_2M_2S_1$, and (**b**) TGA curves of $WC_2M_2S_1$ before and after modification.
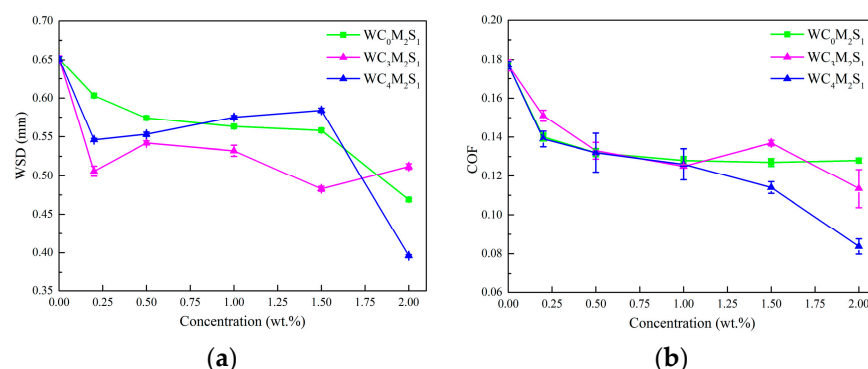
The WSD-concentration and COF-concentration curves for LP containing OA modified MSs (denoted as OAMSs) are presented in Figure 4 for different reaction temperatures and percentages of sodium molybdate dihydrate and thioacetamide. Figure 4a,b show the WSD-concentration and COF-concentration curves for steel balls with lubrication by LP-OAMSs synthesized at different temperatures. In the case of the three lubricants, lower WSDs and COFs were recorded relative to pure LP. Increasing the synthesis temperature to 200 °C resulted in a WSD decrease from 0.65 mm for pure LP to 0.48 mm, and a decrease in COF from 0.178 to 0.121. The steel balls using lubricants containing additives synthesized at 200 °C exhibit better anti-wear and friction reducing ability than observed at other temperatures. Consequently, the synthesis temperature was fixed at 200 °C.
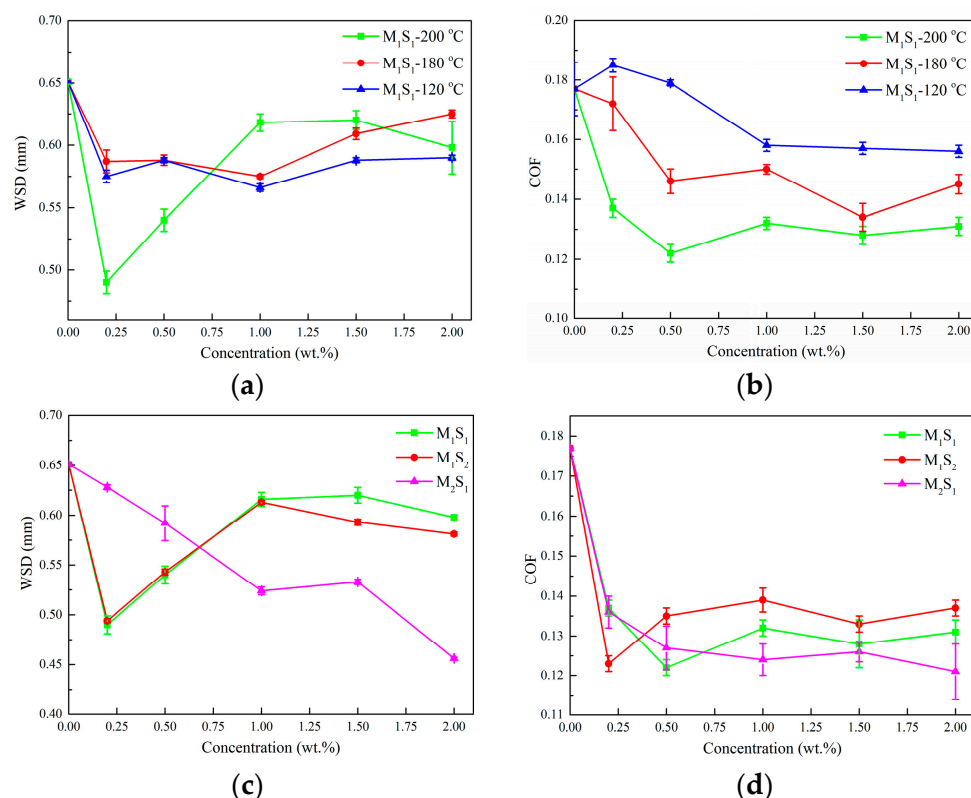
Figure 4. (**a**) WSD concentration curves and (**b**) COF concentration curves of LP-OA-modified M_1S_1 at different reaction temperatures. (**c**) WSD concentration curves and (**d**) COF concentration curves of LP-OA-modified MS with different percentages at 200 °C.

The tribological behavior of MSs with different percentages of sodium molybdate dihydrate and thioacetamide was investigated; the results are presented in Figure 4c,d. As the weights of sodium molybdate dihydrate and thioacetamide were 2 g and 1 g, respectively, the samples are denoted by M_2S_1. The steel balls lubricated with LP-OA-modified M_2S_1 exhibit less friction reduction and anti-wear capability than achieved with the other two lubricants. At a concentration of 2.0 wt.%, a WSD of 0.46 mm was recorded for LP-OAM_2S_1, which is lower than that for LP-M_1S_1 (0.60 mm) and LP-M_1S_2 (0.59 mm), respectively. The weights of sodium molybdate dihydrate and thioacetamide were fixed at 2 g and 1 g, respectively. The non-linearity of COFs with concentrations might be attributed to the changes of viscosity index, adsorption–desorption ability and/or the spread ability of additives in base oil, respectively [25–27].

The WSD concentration curves and COF concentration curves presented in Figure 5a and 5b, respectively, show the results generated for LP-OAWCM_2S_1 using different volumes of willow catkins solution. It can be seen that the steel balls exhibit smaller WSDs for lubrication by LP-OAW$C_3M_2S_1$ with concentrations less than 1.5 wt.% relative to samples without willow catkins. The WSD of steel balls lubricated with LP-OAW$C_3M_2S_1$ at a concentration of 0.2 wt.% is 0.50 mm, which is much smaller than that with LP (0.65 mm) and LP-OAW$C_0M_2S_1$ (0.60 mm). In the case of the COFs of steel balls with LP containing the three additives, there is no marked dependence where use of LP containing the three additives at a concentration of 1.0 wt.% resulted in a COF of 0.121, much lower than that obtained with pure LP (0.178).

Figure 5. (**a**) WSD concentration curves and (**b**) COF concentration curves of LP-OA-modified WCM$_2$S$_1$ with different volumes of Willow catkins solutions.

In a further investigation of the tribological properties of WC$_3$M$_2$S$_1$, urea was added to the solution during hydrothermal reaction (see Figure 6). When 8 g urea was included in the hydrothermal solution, both the WSDs and COFs for the steel balls lubricated with LP-OA modified WC$_3$M$_2$S$_1$ exhibited a marked drop. At a concentration of 0.5 wt.%, a WSD of 0.46 mm was calculated for the balls lubricated with LP containing WC$_3$M$_2$S$_1$ and urea (8 g), which is ca. 70% and 87% of that achieved with pure LP and LP containing WC$_3$M$_2$S$_1$ without urea, respectively. In the case of samples with other amounts of urea (12 g and 4 g), the measured WSDs showed no obvious differences relative to the addition of 8 g urea. Furthermore, the COFs for the balls lubricated with LP containing WC$_3$M$_2$S$_1$ with urea were much lower than lubrication without urea. For example, at a concentration of 0.5 wt.%, a COF of 0.09 mm was recorded for the balls lubricated with LP containing WC$_3$M$_2$S$_1$ with urea (8 g), which is ca. 50% and 69% of that recorded for lubrication with pure LP and LP containing WC$_3$M$_2$S$_1$ without urea, respectively. From an overview of the results, WC$_3$M$_2$S$_1$ with 8 g urea exhibited the lowest coefficients of friction.
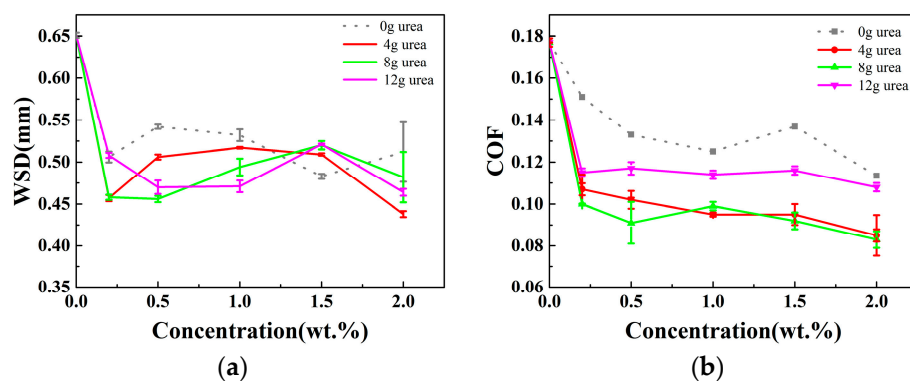
Figure 6. (**a**) WSD concentration and (**b**) COF concentration curves of LP-OA-modified WC$_3$M$_2$S$_1$ with different volumes of urea.

3.2. Discussion

The above experiments serve to demonstrate that the combination of willow catkins and urea can improve the tribological properties of MoS$_2$. Generally speaking, the low friction coefficient of MoS$_2$ was related to its easy sliding between layers under the shearing force of weak van der Waals force between molecular layers. The possible lubrication mechanisms were generally suggested as rolling, deformation, exfoliation-transferring and easier interlayer sliding, and the related factors about improving lubrication performance are also explored. Many reports also suggest that both weak Van der Waals forces between the MoS$_2$ layers and the protective tribo-films containing Mo, S, Fe, C, O and other elements can decrease friction forces and wear rate [7,9,28–31]. For example, Sun et al. synthesized N-doped carbon quantum dots as lubricant additive to investigate the tribological behavior of

MoS$_2$ nanofluid [9]. The tribo-films containing amorphous substances, ultrafine crystalline nanoparticles, and self-lubricating FeSO$_4$/Fe$_2$ (SO$_4$)$_3$ were formed during rotation. Non-equilibrium molecular dynamics simulation results indicated the interaction between S atoms in MoS$_2$ as well as these O- and N-containing functional groups in nitrogen-doped carbon quantum dots with steel surfaces enhanced the stability and strength of tribo-films. Liu studied the tribological properties of coral-like MoS$_2$ as additives of liquid paraffin using four-ball testing machine [30]. The results shows that MoS$_2$ sheets stack randomly under weak Van der Waals force and large layer space can weaken the attractive force, and the nanostructure will be easily distorted, exfoliated and even oxidized during friction. On the other hand, the surface of the steel ball is formed by the boundary lubrication and protective film formed by newly generated Fe-based compounds, molybdenum oxide and other products. So the friction reduction and anti-wear mechanism were focused on the tribo-films and/or the Van der Waals forces.

The morphologies and corresponding elemental analysis of worn surfaces are presented in Figure 7 for lubrication using LP and LP-OA-modified WC$_3$M$_2$S$_1$ with 8 g urea. The WSD of the worn surface using LP-OA modified WC$_3$M$_2$S$_1$ with 8 g urea is 0.45 mm, which is much smaller than the WSD (0.65 mm) using pure LP. The SEM and associated EDXA have revealed that the worn surface of the steel balls lubricated with LP-OA modified WC$_3$M$_2$S$_1$ with urea is smooth with evidence of a Fe, C, O, Mo, S and N content. It should be noted that the percentage of nitrogen on the worn surface increased from 0.06 at.% to 0.92 at.% when 8 g urea was included in the treatment.
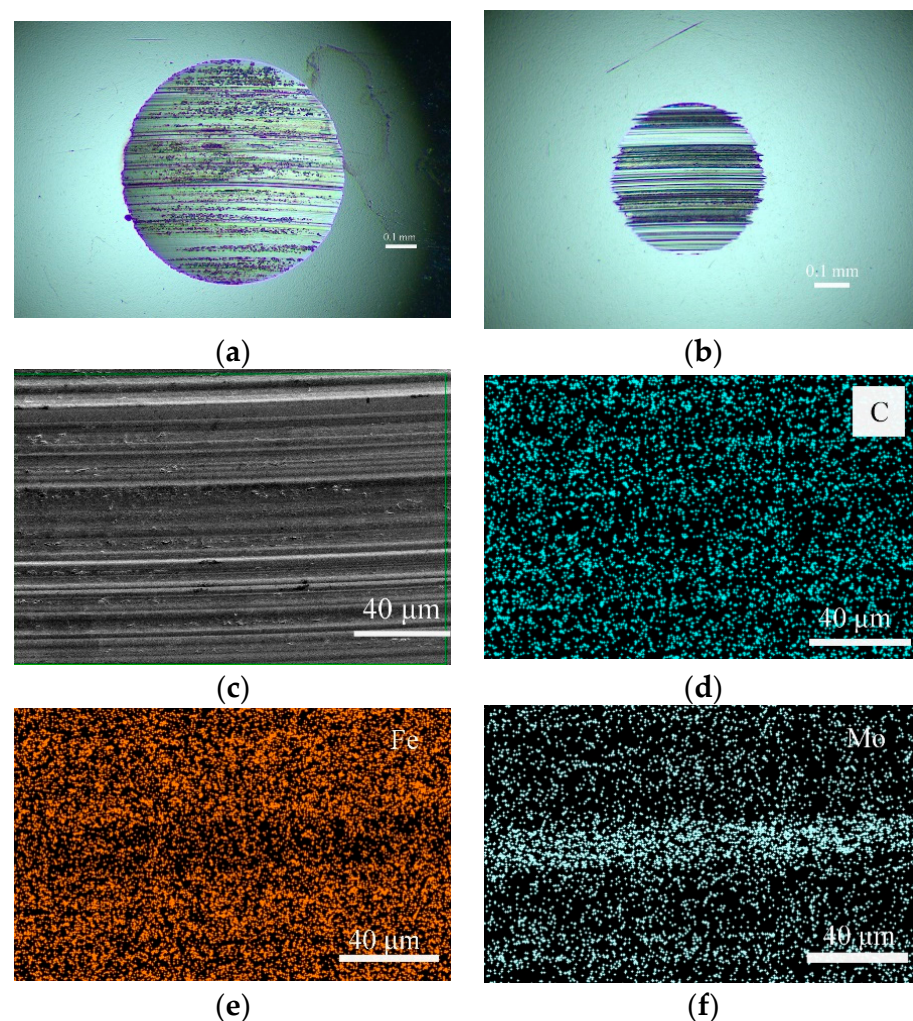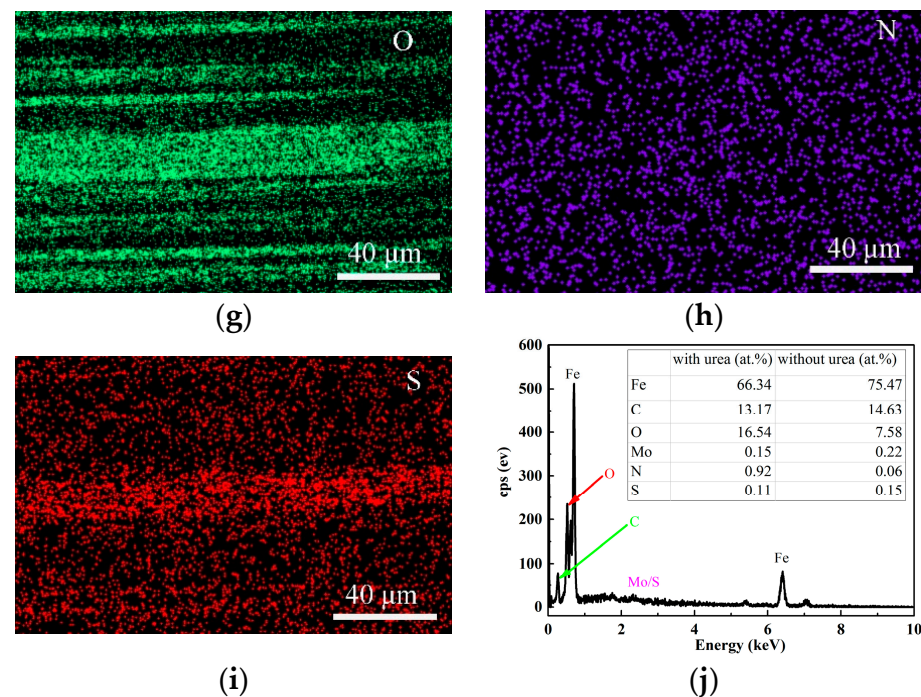

(a)

(b)

(c)

(d)

(e)

(f)

Figure 7. *Cont.*

Figure 7. (**a**) Optical image of the steel ball wear scar following lubrication with LP. (**b**) Optical image, (**c**) SEM image, (**d–i**) EDS element mapping, and (**j**) EDS spectrum of the steel ball wear scar following lubrication with LP containing $WC_3M_2S_1$ with 8 g urea.

The XPS analysis of the worn surfaces following lubrication using LP-$WC_3M_2S_1$, with and without urea, is presented in Figure 8. Peaks due to C1s at 283.1 eV, 284.7 eV, 286.0 eV, and 288.1 eV can be attributed to carbide, carbon, carbon with N/S, and O-C=O, respectively (see Figure 8a and 8g) [19,32]. A comparison of Figure 8g with Figure 8a reveals a greater component of carbide and carbon with N/S on the worn surfaces, which must result from the use of urea during composite treatment. The O1s peaks following lubrication with LP-$WC_3M_2S_1$ are assigned to metal oxides, carbonates, and sulfates [9,19,29]. The signals generated for the worn sample with lubrication using $WC_3M_2S_1$ with urea may be attributed to metal oxides, carbonates and nitrates (see Figure 8b,h) [9,19]. The occurrence of N1s peaks has revealed the formation of nitrides, organic matrix, and azide on the worn surface [9,32]. A consideration of Figure 8c,i suggests the presence of azide on the tribo-film for lubrication with LP containing $WC_3M_2S_1$ with urea. A Mo3d peaks following lubrication with LP-$WC_3M_2S_1$ are attributed to the MoO_3 or $FeMoO_4$ (232.2–235.4 eV), MoS_2 (229.1–232.3 eV), and oxysulfide compound of type MoOxSy (230.7–233.8 eV), respectively (shown as: Figure 8d and 8j) [33]. Furthermore, the weak S2p signal at 161.70 eV and 169.15 eV are due to sulfide and sulfate, respectively, suggesting the presence of FeS, MoS_2 and $FeSO_4$ on the worn surfaces [7,34]. The Fe2p signal was deconvoluted into two peaks at 710.44 eV and 713.04 eV, which may be ascribed to FeS and Fe_2O_3 on the worn surfaces, respectively [7,34]. The results indicate that a tribo-film containing carbon, C-O/N/S, nitride, and sulfide was formed on the worn surfaces during rotation. In the case of the samples lubricated with LP-$WC_3M_2S_1$ and urea, the formation of surface azide, nitride, and FeS may help improve the friction reducing and anti-wear capability of the steel balls.
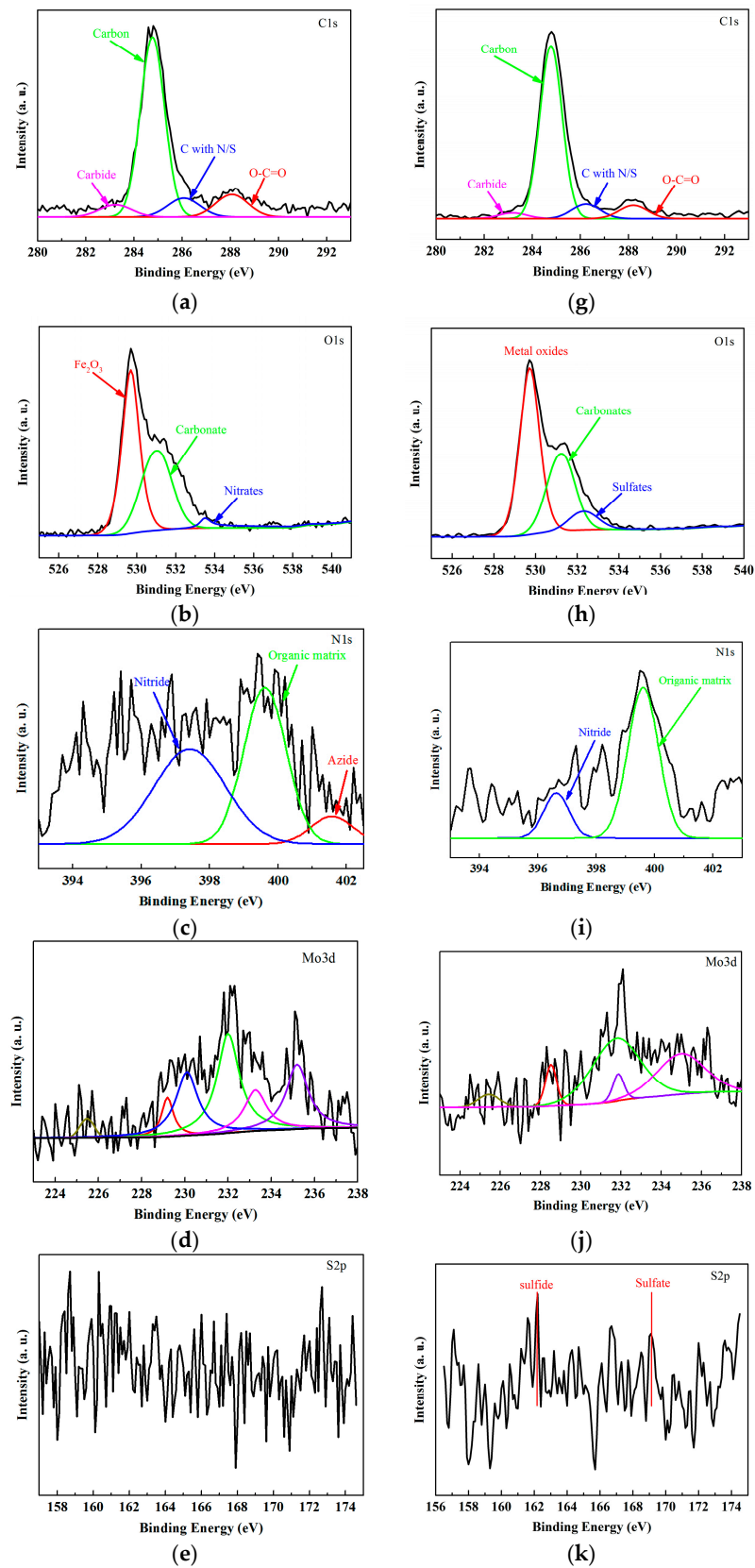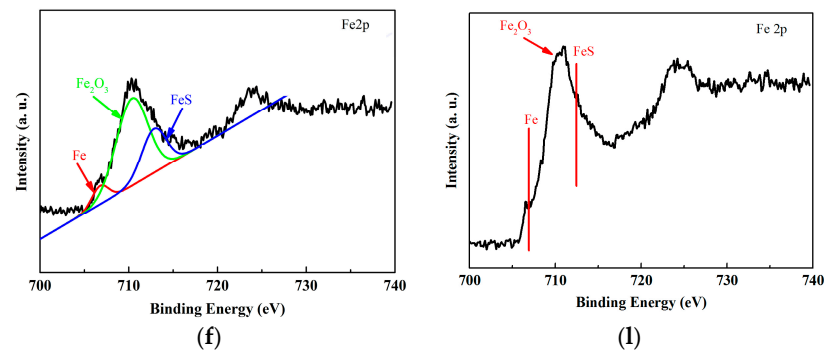
Figure 8. *Cont.*

Figure 8. XPS spectra of the worn surfaces lubricated using LP-WC$_3$M$_2$S$_1$ with (**a–f**) and without (**g–l**) urea.

In order to arrive at a relationship between the wear mechanism and structure of the composites, XRD and the EDXA measurements were conducted for WC$_3$M$_2$S$_1$ with and without urea, and the results are shown in Figure 9. Taking the WC$_3$M$_2$S$_1$ sample, the XRD peaks at 14.10°, 33.32°, 59.02° are attributed to (002), (100), and (008) crystal planes, respectively. In the case of the samples with urea, the 2θ values associated with the (100) and (008) planes were shifted to 32.38° and 57.26°, respectively. The peak due to (002) was split into two peaks at 18.40° and 9.27°, which indicates that graphene-like MoS$_2$ formed due to the inclusion of urea in the solution [35]. The FE-SEM analysis has revealed the presence of loose MoS$_2$ nano-sheets on the samples of WC$_3$M$_2$S$_1$ with urea (Figure 9a). Possibly, the large spaces of these sheets decreased the shearing force of weak van der Waals force between molecular layers and friction coefficient of MoS$_2$ composites. The urea in the solution may decrease the interaction between the solution and MoS$_2$ and increase the inter-layer spacing of the MoS$_2$ nano-sheets [36]. The mapping analysis (shown in Figure S3) and the EDXA spectrum (Figure 9b) have established that the composites contain Mo, S, C, O, and N, where the ratio of Mo to S is 1:2, confirming that MoS$_2$ nano-sheets covered the surfaces of willow catkins. The images and mapping suggest that the MoS$_2$ filled the willow catkins cavity. The nitrogen content increased from 3.84 at.% to 5.5 at.% due to the addition of urea, which suggests that the hybrid of nitrogen with WCMS was formed.
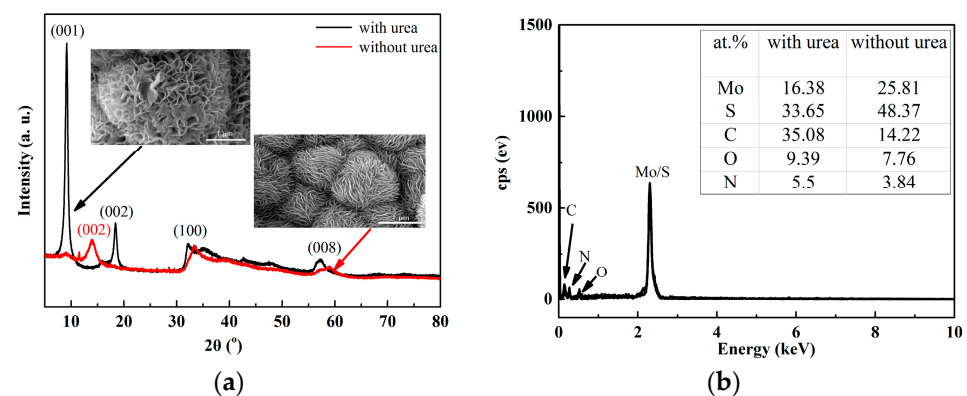

Figure 9. (**a**) XRD pattern and (**b**) EDXA spectra of the WC$_3$M$_2$S$_1$ with and without urea.

The results of the XPS analysis of WC$_3$M$_2$S$_1$ with and without urea are presented in Figure S4. The C1s peaks at ca. 285 eV and 286.1 eV are attributed to free carbon and carbon bonded to nitrogen/oxygen/sulfur, respectively [19,24]. The weak N1s peaks at 407.1 eV, 404.8 eV, 403.7 eV, 400.9 eV, and 401.2 eV are assigned to nitrates, nitrites, the organic matrix, C-NH$_2$, and ammonium salt, respectively [24,31]. Comparing the nitrogen signal for samples with and without urea, the ammonium salt was replaced by organic compounds when urea was added to the solution. The O1s peaks at 533.7 eV, 532.1 eV,

and 530.4 eV are attributed to N-O, S-O, and Mo-O, respectively [24,31]. It is possible that Mo and S on the surface of MoS_2 nano-sheets bonded with oxygen on the surface of hydroxylated willow catkins [34]. Furthermore, the Mo3d and S2p curves have revealed that MoS_2 and MoO_3 were formed, confirming the presence of Mo-O on the nanosheet surface [24,31]. It can be deduced that the MoS_2 sheets were anchored to the hydroxide of the hydroxylated catkins in alkaline solution with the formation of loose MoS_2 [37]. The N_2 adsorption/desorption isotherms (at 77 K) of M_2S_1 and $WC_3M_2S_1$ (presented in Figure S5) have established that the BET surface areas increased from 8.6236 m^2/g to 15.3994 m^2/g as willow catkins were transferred into the composites, which is consistent with the formation of loose composites. Many researchers suggested that ultrathin MoS_2 could significantly improve the lubrication property of oils, because they could be penetrated into the contact area easily [29,30]. Notably, MoS_2 plays an important role in friction reduction and abrasion resistance. Nano-scale MoS_2 possesses high specific surface area, which is more advantageous to be adsorbed on the contact surface. In friction, the shedded MoS_2 flakes can be replenished and updated immediately by other adsorbed MoS_2 film, which plays an important role in lubrication function [30]. Research has shown that the addition of urea to the precursor solution can influence nucleation and growth of crystalline MoS_2, and generate a greater number of loose nano-sheets [38]. These possess weak van der Waals forces of the loose sheets, decreasing the shear forces that the steel balls must overcome, providing effective lubrication during rotation [19].

The above analysis might give some clues of mechanism. First, the lager catkins surface and the significant hydroxide can anchor the MoS_2 sheets with chemical bonds and hinder aggregation of MoS_2 sheets. Second, the addition of urea can generate a significant number of loose nano-sheets and even graphene-like sheets. The weak van der Waals forces between the loose sheets decrease the shear forces of steel balls during rotation, providing effective lubrication. Third, the tribo-film containing MoS_2, FeS, azide, metal oxides and other compounds plays an important role in reducing friction and the anti-wear properties of the composites (see Figure 10).
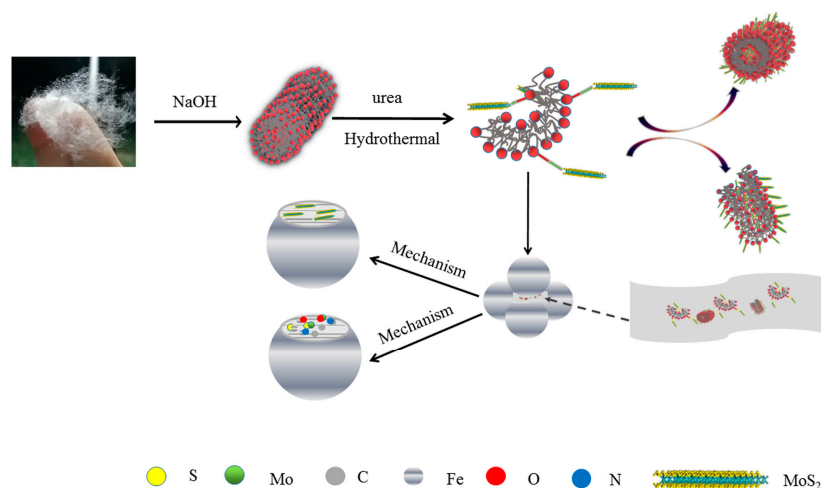
Figure 10. The growth and wear mechanism of WCMS with urea.

4. Conclusions

In this study, willow catkins/MoS_2 nanoparticles have been prepared using a hydrothermal method. By controlling the reaction temperature, the combination of willow catkins and urea can effectively improve tribological properties. The WSD of steel balls lubricated with LP-$OAWC_3M_2S_1$ at a concentration of 0.2 wt.% is 0.50 mm, which is much smaller than that with LP (0.65 mm) and LP-$OAWC_0M_2S_1$ (0.60 mm), respectively. At a concentration of 0.5 wt.%, the WSD and COF of steel balls when lubricated using LP containing modified $WC_3M_2S_1$ with urea (8g) were 0.46 mm and 0.09, representing ca. 70% and 50% of that observed for lubrication with pure LP, respectively. The tribo-film

contained MoS_2, FeS, azide, metal oxides and other compounds that play an important role in reducing friction and the anti-wear properties of the composites. The catkins surface contains a significant hydroxide component that serves to anchor the MoS_2 sheets and hinder aggregation of MoS_2. The addition of urea to the precursor solution can alter the nucleation and growth of crystalline MoS_2, generating a significant number of loose nano-sheets and even graphene-like sheets. The weak van der Waals forces between the loose sheets decrease the shear forces of steel balls during rotation, providing effective lubrication.

Supplementary Materials: The following supporting information can be downloaded at https://www.mdpi.com/article/10.3390/lubricants11120524/s1. Figure S1. The stability of lubricants with additives. Figure S2. The mapping analysis of the $WC_2M_2S_1$s with the hydrothermal temperature of 200 °C. Figure S3. The mapping analysis of the $WC_2M_2S_1$s with urea at a hydrothermal temperature of 200 °C. Figure S4. The XPS spectra of the $WC_3M_2S_1$ with (a–e) and without (f–j) urea. Figure S5. N_2 adsorption/desorption isotherms (77K) of M_2S_1s (A) and $WC_3M_2S_1$s (B), respectively. Table S1. The catalogue and component content of the composites.

Data Availability Statement: Data are contained within the article.

Conflicts of Interest: Author Yungang Bai was employed by the company Shandong Qichanxintu Composite Material Co., Ltd., China. The remaining authors declare that the research was conducted in the absence of any commercial or financial relationships that could be construed as a potential conflict of interest.

References

1. Kumari, S.; Chouhan, A.; Konathala, L.S.K.; Sharma, O.P.; Ray, S.S.; Ray, A.; Khatri, O.P. Chemically functionalized 2D/2D hexagonal boron nitride/molybdenum disulfide heterostructure for enhancement of lubrication properties. *Appl. Surf. Sci.* **2022**, *579*, 152157. [CrossRef]
2. Zhang, W.; Demydov, D.; Jahan, M.P.; Mistry, K.; Erdemir, A.; Malshe, A.P. Fundamental understanding of the tribological and thermal behavior of Ag-MoS_2 nanoparticle-based multi-component lubricating system. *Wear* **2012**, *288*, 9–16. [CrossRef]
3. Su, Y.; Zhang, Y.; Song, J.; Hu, L. Novel approach to the fabrication of an alumina-MoS_2 self-lubricating composite via the in situ synthesis of nanosized MoS_2. *ACS Appl. Mater Interfaces* **2017**, *9*, 30263–30266. [CrossRef] [PubMed]
4. Pan, S.; Jin, K.; Wang, T.; Zhang, Z.; Zheng, L.; Umehara, N. Metal matrix nanocomposites in tribology: Manufacturing, performance, and mechanisms. *Friction* **2022**, *10*, 1596–1634. [CrossRef]
5. Coleman, J.N.; Lotya, M.; O'Neill, A.; Bergin, S.D.; King, P.J.; Khan, U.; Young, K.; Gaucher, A.; De, S.; Smith, R.J.; et al. Two-dimensional nanosheets produced by liquid exfoliation of layered materials. *Science* **2011**, *331*, 568–571. [CrossRef]
6. Nicolosi, V.; Chhowalla, M.; Kanatzidis, M.G.; Strano, M.S.; Coleman, J.N. Liquid exfoliation of layered materials. *Science* **2013**, *340*, 1226419. [CrossRef]
7. Gong, K.; Lou, W.; Zhao, G.; Wu, X.; Wang, X. MoS_2 nanoparticles grown on carbon nanomaterials for lubricating oil additives. *Friction* **2021**, *9*, 747–757. [CrossRef]
8. Qiu, S.; Hu, Y.; Shi, Y.; Hou, Y.; Kan, Y.; Chu, F.; Sheng, H.; Yuen, R.K.; Xing, W. In situ growth of polyphosphazene particles on molybdenum disulfide nanosheets for flame retardant and friction application. *Compos. Part A Appl. Sci. Manuf.* **2018**, *114*, 407–417. [CrossRef]
9. He, J.; Sun, J.; Choi, J.; Wang, C.; Su, D. Synthesis of N-doped carbon quantum dots as lubricant additive to enhance the tribological behavior of MoS_2 nanofluid. *Friction* **2023**, *11*, 441–459. [CrossRef]

10. Zheng, X.; Xu, Y.; Geng, J.; Peng, Y.; Olson, D.; Hu, X. Tribological behavior of Fe_3O_4/MoS_2 nanocomposites additives in aqueous and oil phase media. *Tribol. Int.* **2016**, *102*, 79–87. [CrossRef]

11. Wang, K.; Zhao, N.; Lei, S.; Yan, R.; Tian, X.; Wang, J.; Song, Y.; Xu, D.; Guo, Q.; Liu, L. Promising biomass-based activated carbons derived from willow catkins for high performance supercapacitors. *Electrochim. Acta* **2015**, *166*, 1–11. [CrossRef]

12. Zhang, S.; Zang, L.; Dou, T.; Zou, J.; Zhang, Y.; Sun, L. Willow catkins-derived porous carbon membrane with hydrophilic property for efficient solar steam generation. *ACS Omega* **2020**, *5*, 2878–2885. [CrossRef] [PubMed]

13. Wang, M.; Zhou, J.; Wu, S.; Wang, H.; Yang, W. Green synthesis of capacitive carbon derived from platanus catkins with high energy density. *J. Mater. Sci. Mater. Electron.* **2019**, *30*, 4184–4195. [CrossRef]

14. Yan, Y.; Fan, C.; Yang, Y.; Xie, Y.; Cao, Y.; Lin, J.; Zou, Y.; You, C.; Xu, Y.; Yang, R. Effects of structural feature of biomass raw materials on carbon products as matrix in cathode of Li-S battery and its electrochemical performance. *Ionics* **2020**, *26*, 6035–6047. [CrossRef]

15. Tong, M.; Cao, B.; Li, Y.; Chen, L.; Fu, Y. Biomass carbon combined antimony sulfide with various contents as anodes with improved cycle stability in the sodium ion batteries. *J. Alloys Compd.* **2023**, *936*, 168270. [CrossRef]

16. Gouda, M.S.; Shehab, M.; Helmy, S.; Soliman, M.; Salama, R.S. Nickel and cobalt oxides supported on activated carbon derived from willow catkin for efficient supercapacitor electrode. *J Energy Storage* **2023**, *61*, 106806. [CrossRef]

17. Zhao, D.; Wang, L.; Qiu, M.; Zhang, N. Amorphous Se restrained by biomass-derived defective carbon for stable Na-Se batteries. *ACS Appl. Energy Mater.* **2021**, *4*, 7219–7225. [CrossRef]

18. Song, L.; Chang, J.; Ma, Y.; Jiang, W.; Xu, Y.; Liang, C.; Chen, Z.; Zhang, Y. Biomass-derived nitrogen and sulfur co-doped carbon microtubes for the oxygen reduction reaction. *Mater. Chem. Front.* **2020**, *4*, 3251–3257. [CrossRef]

19. Zang, C.; Yang, M.; Liu, E.; Qian, Q.; Zhao, J.; Zhen, J.; Zhang, R.; Jia, Z.; Han, W. Synthesis, characterization and tribological behaviors of hexagonal boron nitride/copper nanocomposites as lubricant additives. *Tribol. Int.* **2022**, *165*, 107312. [CrossRef]

20. Li, W.; Yan, Z.; Shen, D.; Zhang, Z.; Yang, R. Microstructures and tribological properties of MoS_2 overlayers on MAO Al alloy. *Tribol. Int.* **2023**, *1181*, 108348. [CrossRef]

21. Sarwar, S.; Karamat, S.; Bhatti, A.S.; Aydinol, M.K.; Oral, A.; Hassan, M.U. Synthesis of graphene-MoS_2 composite based anode from oxides and their electrochemical behavior. *Chem. Phys. Lett.* **2021**, *781*, 138969. [CrossRef]

22. Shen, P.; Yang, X.; Du, M.; Zhang, H. Temperature and laser-power dependent Raman spectra of MoS_2/RGO hybrid and few-layered MoS_2. *Phys. B Condens. Matter* **2021**, *604*, 412693. [CrossRef]

23. Xuan, D.; Zhou, Y.; Nie, W.; Chen, P. Sodium alginate-assisted exfoliation of MoS_2 and its reinforcement in polymer nanocomposites. *Carbohydr. Polym.* **2017**, *155*, 40–48. [CrossRef] [PubMed]

24. Mall, V.K.; Ojha, R.P.; Tiwari, P.; Prakash, R. Immunosuppressive drug sensor based on MoS_2-polycarboxyindole modified electrodes. *Results Chem.* **2022**, *4*, 100345. [CrossRef]

25. Hirayama, S.; Kurokawa, T.; Gong, J.P. Non-linear rheological study of hydrogel sliding friction in water and concentrated hyaluronan solution. *Tribol. Int.* **2020**, *147*, 106270. [CrossRef]

26. Sharma, A.K.; Katiyar, J.K.; Bhaumik, S.; Roy, S. Influence of alumina/MWCNT hybrid nanoparticle additives on tribological properties of lubricants in turning operations. *Friction* **2019**, *7*, 153–168. [CrossRef]

27. Mousavi, S.B.; Heris, S.Z.; Estellé, P. experimental comparison between ZnO and MoS_2 nanoparticles as additives on performance of diesel oil-based nano lubricant. *Sci. Rep.* **2020**, *10*, 5813. [CrossRef]

28. Guimarey, M.J.; Viesca, J.L.; Abdelkader, A.M.; Thomas, B.; Battez, A.H.; Hadfield, M. Electrochemically exfoliated graphene and molybdenum disulfide nanoplatelets as lubricant additives. *J. Mol. Liq.* **2021**, *342*, 116959. [CrossRef]

29. Chen, J.; Xu, Z.; Hu, Y.; Yi, M. PEG-assisted solvothermal synthesis of MoS_2 nanosheets with enhanced tribological property. *Lubr. Sci.* **2020**, *32*, 273–282. [CrossRef]

30. Liu, L.; Huang, Z.; Huang, P. Fabrication of coral-like MoS_2 and its application in improving the tribological performance of liquid paraffin. *Tribol. Int.* **2016**, *104*, 303–308. [CrossRef]

31. Wu, X.; Gong, K.; Zhao, G.; Lou, W.; Wang, X.; Liu, W. Surface modification of MoS_2 nanosheets as effective lubricant additives for reducing friction and wear in poly-α-olefin. *Ind. Eng. Chem. Res.* **2018**, *57*, 8105–8114. [CrossRef]

32. Kathiravan, D.; Huang, B.R.; Saravanan, A.; Prasannan, A.; Hong, P.D. Highly enhanced hydrogen sensing properties of sericin-induced exfoliated MoS_2 nanosheets at room temperature. *Sens. Actuators B Chem.* **2019**, *279*, 138–147. [CrossRef]

33. Garcia, I.; Galipaud, J.; Kosta, I.; Grande, H.; Garcia-Lecina, E.; Dassenoy, F. Influence of the organic moiety on the tribological properties of MoS_2: Glycol hybrid nanoparticles-based dispersions. *Tribol. Int.* **2020**, *68*, 104. [CrossRef]

34. Xu, W.; Fu, C.; Hu, Y.; Chen, J.; Yang, Y.; Yi, M. Synthesis of hollow core-shell MoS_2 nanoparticles with enhanced lubrication performance as oil additives. *Bull. Mater. Sci.* **2021**, *44*, 88. [CrossRef]

35. Chen, T.; Xia, Y.; Jia, Z.; Liu, Z.; Zhang, H. Synthesis, characterization, and tribological behavior of oleic acid capped graphene oxide. *J. Nanomater.* **2014**, *2014*, 654145. [CrossRef]

36. Pal, K.; Majumder, T.P.; Schirhagl, R.; Ghosh, S.; Roy, S.K.; Dabrowski, R. Efficient one-step novel synthesis of ZnO nanospikes to nanoflakes doped OAFLCs (W-182) host: Optical and dielectric response. *Appl. Surf. Sci.* **2013**, *280*, 405–417. [CrossRef]

37. Liu, J.; Zhao, S.; Wang, C.; Ma, Y.; He, L.; Liu, B.; Zhang, Z. Catkin-derived mesoporous carbon-supported molybdenum disulfide and nickel hydroxyl oxide hybrid as a bifunctional electrocatalyst for driving overall water splitting. *J. Colloid Interface Sci.* **2022**, *608*, 1627–1637. [CrossRef]

38. Liu, Y.; Li, X.; Liu, T.; Zheng, Z.; Liu, Q.; Wang, Y.; Qin, Z.; Guo, H.; Liang, Y. Alcohols assisted in-situ growth of MoS_2 membrane on tubular ceramic substrate for nanofiltration. *J. Membr. Sci.* **2022**, *659*, 120777. [CrossRef]